ORIGINAL RESEARCH

Peroxisome Proliferator–activated Receptor-γ Deficiency Exacerbates Fibrotic Response to Mycobacteria Peptide in Murine Sarcoidosis Model

Anagha Malur[1]*, Arjun Mohan[1]*, Robert A. Barrington[2], Nancy Leffler[1], Amrita Malur[1], Barbara Muller-Borer[3], Gina Murray[4], Kim Kew[5], Chuanzhen Zhou[6], Josh Russell[7], Jacob L. Jones[7], Christopher J. Wingard[8], Barbara P. Barna[1], and Mary Jane Thomassen[1]

[1]Program in Lung Cell Biology and Translational Research, Division of Pulmonary, Critical Care and Sleep Medicine, [3]Department of Engineering, [4]Department of Pathology, and [5]Department of Chemistry, East Carolina University, Greenville, North Carolina; [2]Department of Microbiology and Immunology, University of South Alabama, Mobile, Alabama; [6]Analytical Instrumentation Facility and [7]Department of Materials Science and Engineering, North Carolina State University, Raleigh, North Carolina; and [8]Department of Physical Therapy, School of Movement and Rehabilitation Sciences, College of Health Professions, Bellarmine University, Louisville, Kentucky

ORCID IDs: 0000-0001-5713-5369 (R.A.B.); 0000-0002-4817-5323 (B.M.-B.); 0000-0002-0400-0433 (K.K.); 0000-0002-9353-7231 (C.Z.); 0000-0002-8251-5678 (C.J.W.); 0000-0003-1229-7668 (M.J.T.).

Abstract

We established a murine model of multiwall carbon nanotube (MWCNT)-elicited chronic granulomatous disease that bears similarities to human sarcoidosis pathology, including alveolar macrophage deficiency of peroxisome proliferator–activated receptor γ (PPARγ). Because lymphocyte reactivity to mycobacterial antigens has been reported in sarcoidosis, we hypothesized that addition of mycobacterial ESAT-6 (early secreted antigenic target protein 6) to MWCNT might exacerbate pulmonary granulomatous pathology. MWCNTs with or without ESAT-6 peptide 14 were instilled by the oropharyngeal route into macrophage-specific PPARγ-knockout (KO) or wild-type mice. Control animals received PBS or ESAT-6. Lung tissues, BAL cells, and BAL fluid were evaluated 60 days after instillation. PPARγ-KO mice receiving MWCNT + ESAT-6 had increased granulomas and significantly elevated fibrosis (trichrome staining) compared with wild-type mice or PPARγ-KO mice that received only MWCNT. Immunostaining of lung tissues revealed elevated fibronectin and Siglec F expression on $CD11c^+$ infiltrating alveolar macrophages in the presence of MWCNT + ESAT-6 compared with MWCNT alone. Analyses of BAL fluid proteins indicated increased levels of transforming growth factor (TGF)-β and the TGF-β pathway mediator IL-13 in PPARγ-KO mice that received MWCNT + ESAT-6 compared with wild-type or PPARγ-KO mice that received MWCNT. Similarly, mRNA levels of matrix metalloproteinase 9, another requisite factor for TGF-β production, was elevated in PPARγ-KO mice by MWCNT + ESAT-6. Analysis of ESAT-6 in lung tissues by mass spectrometry revealed ESAT-6 retention in lung tissues of PPARγ-KO but not wild-type mice. These data indicate that PPARγ deficiency promotes pulmonary ESAT-6 retention, exacerbates macrophage responses to MWCNT + ESAT-6, and intensifies pulmonary fibrosis. The present findings suggest that the model may facilitate understanding of the effects of environmental factors on sarcoidosis-associated pulmonary fibrosis.

Keywords: multiwall carbon nanotubes; granuloma; peroxisome proliferator–activated receptor-γ fibrosis; lung; sarcoid

Charting the relationship between environmental carbon pollutants and human disease is a continuing problem (1). Combustion-generated carbonaceous pollutants are found throughout the environment and can include multiwall carbon nanotubes (MWCNT) or nanoparticles (reviewed by Lam and colleagues [2]). Carbon nanotubes (CNTs) are cylindrically shaped, high-aspect ratio, carbon-based nanostructures. MWCNTs are a type of CNT that consists of multiple

(Received in original form October 22, 2018; accepted in final form February 11, 2019)

*These authors contributed equally to this work.

Supported by National Institutes of Health (NIH) grant ES025191 (M.J.T.) and NIH Center for Human Health and the Environment grant P30 ES025128.

Author Contributions: Anagha Malur, A. Mohan, R.A.B., B.P.B., and M.J.T.: concept and design; N.L., Amrita Malur, K.K., C.Z., and J.R.: acquisition of data; Anagha Malur, A. Mohan, B.M.-B., G.M., J.L.J., B.P.B., and M.J.T.: analysis and interpretation; and Anagha Malur, A. Mohan, C.J.W., B.P.B., and M.J.T.: drafting of manuscript for important intellectual content.

Correspondence and requests for reprints should be addressed to Mary Jane Thomassen, Ph.D., Division of Pulmonary and Critical Care Medicine, East Carolina University, 3E-149 Brody Medical Sciences Building, Greenville, NC 27834. E-mail: thomassenm@ecu.edu.

This article has a data supplement, which is accessible from this issue's table of contents at www.atsjournals.org.

Am J Respir Cell Mol Biol Vol 61, Iss 2, pp 198–208, Aug 2019

Originally Published in Press as DOI: 10.1165/rcmb.2018-0346OC on February 11, 2019
Internet address: www.atsjournals.org

overlapping layers of carbon around the cylinder. CNTs are on the scale of tens of nanometers in diameter and can be very long (e.g., >1 μm) (2). CNTs have been reported in dusts resulting from the intense combustion associated with the 2001 World Trade Center disaster as well as in lung tissues of World Trade Center–exposed individuals diagnosed with sarcoidosis (3). More recently, CNTs have been found in diesel exhausts and in lung tissues of urban Parisian children (4). Studies of CNTs in laboratory animals have demonstrated both granulomatous and fibrotic lung pathology, depending on nanotube configuration and dose (5, 6).

In sarcoidosis, a human granulomatous disease of unknown etiology primarily affecting the lungs, epidemiological studies have suggested linkage with multiple environmental risk factors, including exposure to conditions under which CNTs may be produced (7–9). To investigate the potential role of CNTs in pulmonary disease, we used oropharyngeal instillation of MWCNT to construct a murine model of granulomatous disease (10). Strikingly, our previous publications have shown that the MWCNT mouse model mirrors several characteristics found in patients with pulmonary sarcoidosis, including chronicity of granulomatous pathology and a deficiency in alveolar macrophage expression of the lipid-regulatory transcription factor peroxisome proliferator–activated receptor γ (PPARγ) (11–13).

Adaptive immune responses to mycobacterial proteins have been implicated in sarcoidosis immunopathology (14), and we previously examined the effects of instilling a mycobacterial peptide of ESAT-6 (early secreted antigenic target protein 6) together with MWCNT in C57BL/6 wild-type mice (15). ESAT-6 peptide 14 was specifically chosen because it appears to be the only ESAT-6 peptide to elicit significant immune responses in lymphocytes from patients with sarcoidosis (16). Addition of ESAT-6 to MWCNT elicited a mild fibrotic response in wild-type mice (15). In the present study, we used macrophage-specific PPARγ-knockout (KO) mice, which, compared with wild-type mice, display elevated lymphocytes and granulomatous pathology in response to instilled MWCNT (17). We have also noted that untreated PPARγ-KO mice exhibit endogenous T-helper cell type 1 (Th1)-type inflammatory responses (18). Because PPARγ deficiency, elevated lymphocytes, and Th1-type responses are all characteristics reported in sarcoidosis, we hypothesized that the combined instillation of ESAT-6 and MWCNT into PPARγ-KO mice might generate a more intensive pathology that would more closely resemble that reported in sarcoidosis.

Methods

MWCNT Model

All studies were conducted in conformity with Public Health Service policy on humane care and use of laboratory animals and were approved by the institutional animal care committee at East Carolina University, Animal Use Protocol J199. C57BL/6J wild-type (The Jackson Laboratory) or macrophage-specific PPARγ-KO mice (18) received oropharyngeal instillation of MWCNT. MWCNTs (900-1501, lot-GS1802; SES Research) were freshly prepared and have previously been described extensively (10). A single pulmonary instillation of MWCNT (100 μg) in PBS/35% surfactant (Ony Inc. [vehicle] ± ESAT-6 peptide 14 [NNALQNLARTISEAG] 20 μg) were delivered to wild-type mice and PPARγ-KO mice. Sham control animals received vehicle; additional control animals received ESAT-6. Animals were killed at 60 days after instillation and evaluated as previously described (17).

Characterization of BAL Cells

BAL cells were obtained as previously described (18) and in the data supplement.

Protein Analyses of BAL Fluids

Proteins were assayed in BAL fluid (BALF) for transforming growth factor (TGF)-β (BioLegend), platelet-derived growth factor subunit A (PDGFa) (RayBiotech), and IL-13 (R&D Systems).

Histological Analysis

Lungs were dissected and fixed in PBS-buffered 10% formalin and embedded in paraffin. A semiquantitative scoring system previously described (17) was used for a relative comparison of the numbers and quality of the granulomas formed in mice that received MWCNT versus ESAT-6 + MWCNT (*see* data supplement). For determination of fibrosis, 5-μm sections were stained with Masson's trichrome (Provia Diagnostics). Fibrosis was quantified using a modified Ashcroft scale as described by Hübner and colleagues (19). For each condition, six lung sections were scored. Scores by two investigators were averaged for final analysis.

Immunohistochemistry

Frozen lung tissue sections (7 μm) were fixed with 4% paraformaldehyde–PBS, permeabilized with Triton X-100, blocked with normal goat serum in PBS/Triton X-100 for nonspecific binding, and stained with antifibronectin (Fn1) antibody(ab45688; Abcam) or anti-CD3 antibody (ab5690; Abcam) at 1:100 dilution, followed by Alexa Fluor–conjugated goat antirabbit IgG (Invitrogen). Slides were counterstained with DAPI (Vector Laboratories) to facilitate nuclear localization. For Siglec F and CD11c staining, tissue sections were fixed with acetone and blocked with Fcr blocking reagent. Siglec F phycoerythrin antibody (552126; BD Pharmingen) was used at 1:200 dilution, and CD11c biotinylated (13-0114; Affymetrix) was used at 1:200 dilution with a streptavidin–fluorescein isothiocyanate antibody (Invitrogen).

Mass Spectrometry

Optima grade methanol, acetonitrile, formic acid, and water were purchased from Fisher Scientific. Lung tissue weights were recorded and added to a 15-ml centrifuge tube. Methanol (500 μl) with 0.2% formic acid was added to the tissue and homogenized using an ultrasonic probe. Samples were homogenized for approximately 20 seconds on ice, incubated at −20°C for 1 hour, and centrifuged at 1,000 rpm. The supernatant was placed in a microcentrifuge tube and centrifuged for 20 minutes at 4°C. Samples were placed in an autosampler vial for analysis by nano liquid chromatography–mass spectrometry (nano-LC/MS).

Statistical Analyses

Data were analyzed by Student's *t* test or one-way ANOVA and Tukey's test using Prism 7 software (GraphPad Software, Inc.).

Results

Characterization of MWCNT with and without ESAT-6

Scanning electron microscopy (SEM) and subsequent characterization of MWCNTs

are shown in Figures E1A and E1B in the data supplement. The SEM images of the MWCNTs were analyzed, and the distributions of the MWCNTs' widths are shown in Figure E1B; the highest-frequency width is near 20–30 nm. An effective particle size can be calculated for larger volumes of MWCNTs, and this particle size represents an average of the length of the MWCNTs in all dimensions (i.e., lying somewhere between the small widths of 20–30 nm and the lengths up to microns). This distribution before addition of ESAT-6 (Figure E1C) is unimodal with the mode (highest frequency) near 150 nm. This value in the PBS-only condition correlates well as an effective average size of the nanotubes shown in Figure E1A. After addition of ESAT-6, the distribution becomes bimodal with a substantially larger mode appearing around 1,500 nm. As demonstrated in Figure E1C, the value of the particle size distribution measurements is the ability to characterize how the MWCNTs disperse in different media.

The zeta potentials of the solutions containing PBS and PBS with ESAT-6 were −10.9 mV (±2) and −0.6 mV (±2.6), respectively. The zeta potential change after addition of ESAT-6 shows that the surface potential of the CNTs is affected, and this may contribute to potential agglomeration and the appearance of the larger mode in the particle size distribution. Chemical and phase analysis was performed using time-of-flight secondary ion mass spectrometry (TOF-SIMS) and X-ray diffraction (XRD). The XRD shows that the CNTs possess the expected primary phase with a small secondary phase present. TOF-SIMS confirmed that the secondary phase consists of an Mo-containing species, and phase identification using XRD indicates that this phase is likely MoC. The fraction of the secondary phase is low (∼2 wt% or less). The Raman spectra shown in Figure E1D are consistent with the MWCNT structure, specifically the observation of the G band at 1,567 cm^{-1} and the disorder-induced Raman peaks at 1,341 cm^{-1} (D band) and 2,676 cm^{-1} (2D band). The presence of the D bands indicates disorder present in the CNT structures.

The MWCNTs used in the present study have both similar and different features relative to the MWCNTs used by Huizar and colleagues (10). The sizes, morphologies, and primary phases of the two MWCNT batches are similar, as shown by SEM, diameter analysis, size distribution measurements, XRD, and Raman spectroscopy. The XRD and TOF-SIMS results show that a small amount of a secondary phase is present, consisting of the element Mo and likely the MoC phase. XRD and TOF-SIMS were repeated on the MWCNT batch used by Huizar and colleagues (10 and results not shown), and these impurities were not observed in the previous MWCNT batch. X-ray photoelectron spectroscopy of both batches (results not shown) does not indicate evidence of Mo, but TOF-SIMS is more sensitive to trace elements than X-ray photoelectron spectroscopy. The Mo impurity is different from the primary Fe impurity observed by Huizar and colleagues (10). The addition of ESAT-6 to the solution influences the zeta potential, which affects the size distribution. Specifically, a small amount of MWCNT agglomeration may occur with ESAT-6 addition.

Table 1. Granuloma Score in Peroxisome Proliferator–activated Receptor γ–Knockout Mice

MWCNT	MWCNT + ESAT-6
3.8 ± 0.3 *n* = 12	5.5 ± 0.2 *n* = 6

Definition of abbreviations: ESAT-6 = early secreted antigenic target protein 6; MWCNT = multiwall carbon nanotube.

Addition of ESAT-6 to MWCNT Intensifies Granuloma Formation and Fibrosis in PPARγ-KO Mice

Previously, we reported that MWCNT-induced granulomas were elevated in PPARγ-KO mice compared with wild type (10). In the present study, we investigated the effect of ESAT-6 on

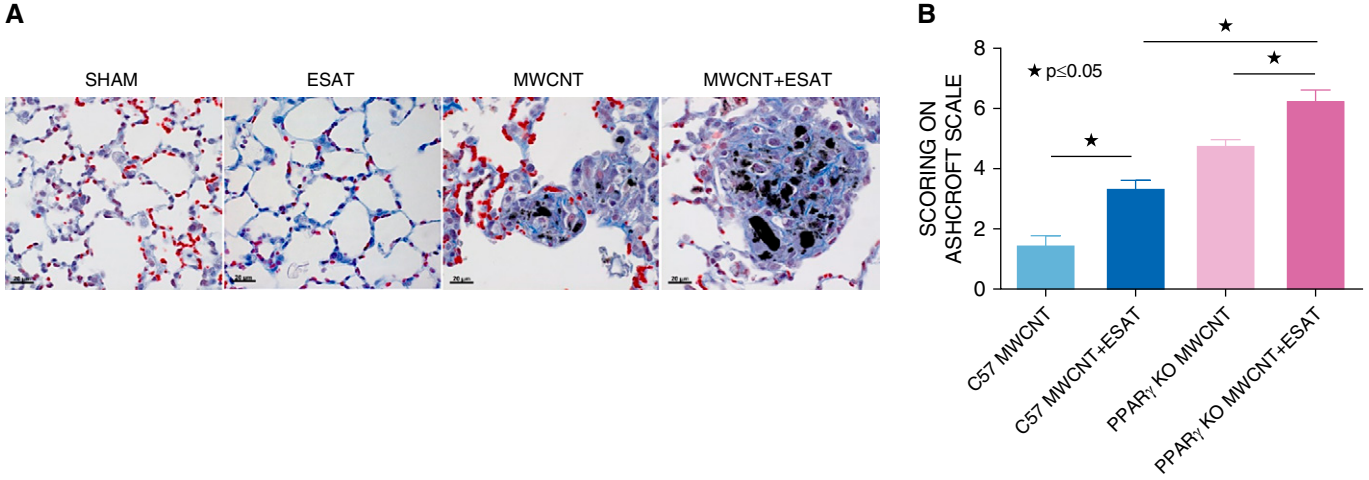

Figure 1. ESAT-6 (early secreted antigenic target protein 6) exacerbates granulomas and fibrosis in mice instilled with MWCNT or MWCNT + ESAT-6 or PBS for 60 days (60-day mice). (*A*) Representative light micrographs illustrating that granuloma formation in MWCNT + ESAT-6–instilled mice after 60 days is increased compared with mice instilled with MWCNT alone. As indicated by trichrome staining, fibrosis is increased in the areas around granulomas as well as within granulomas. Scale bars: 20 μm. (*B*) Modified Ashcroft scoring of fibrosis. In peroxisome proliferator–activated receptor γ–knockout (PPARγ–KO) mice 60 days after instillation with MWCNT + ESAT-6, fibrosis is increased compared with mice instilled with MWCNT alone and also compared with C57BL/6 wild-type mice instilled with MWCNT + ESAT-6. Reported are the mean ± SEM values of two independent observers from six lungs for each group. ★$P \leq 0.05$. MWCNT = multiwall carbon nanotube.

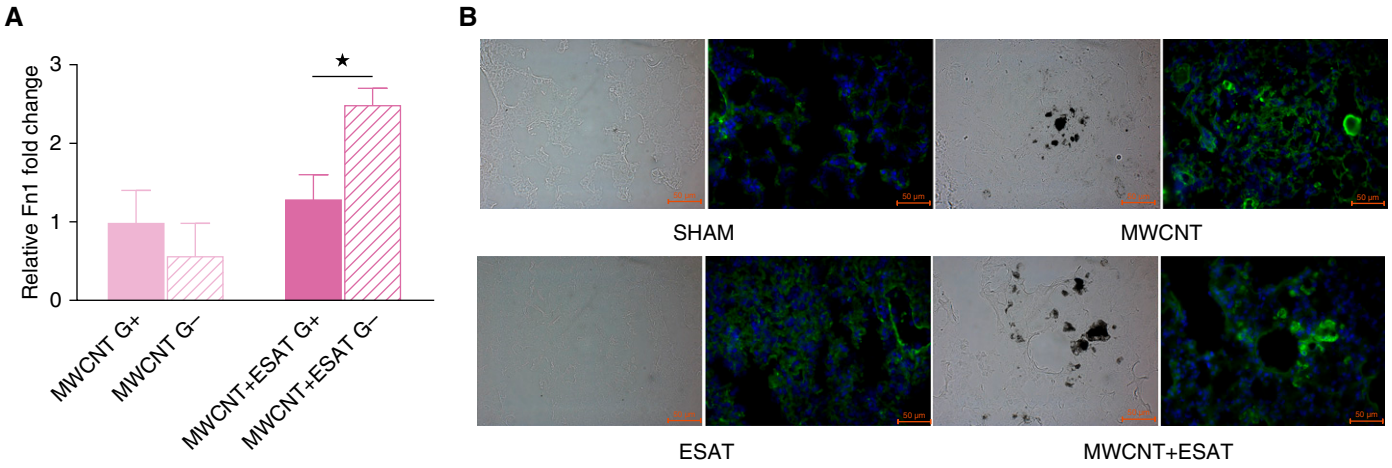

Figure 2. ESAT-6 increases fibronectin (Fn1) in 60-day PPARγ-KO mice. (*A*) Laser capture microdissection from lungs of 60-day PPARγ-KO mice instilled with MWCNT + ESAT-6 shows increased expression of fibronectin mRNA in granuloma-positive and granuloma-negative regions compared with lungs instilled with only MWCNT. Reported are the mean ± SEM values for four different lungs. (*B*) Representative bright-field and immunofluorescence staining for fibronectin indicates low levels in mice instilled with sham fluid and ESAT-6 alone but increased fibronectin protein around granulomas in both MWCNT- and MWCNT + ESAT-6–instilled animals. The dark-appearing material in the bright-field images is the accumulation of MWCNT in the tissue. Scale bars: 50 μm. ★$P \leq 0.05$.

MWCNT-induced granulomas in PPARγ-KO mice at 60 days after instillation. The results indicated that MWCNT + ESAT-6 elicited a significantly ($P \leq 0.05$) higher histologic score (17) than MWCNT alone at 60 days (Table 1). Interestingly, the 60-day effect was similar to that noted previously in C57BL/6 wild-type mice exposed to MWCNT + ESAT-6 (15). No granulomas were detected in PPARγ-KO mice receiving sham treatment or ESAT-6 alone.

Fibrotic changes were apparent in 60-day lung sections stained with Masson's trichrome, both within the granulomas and in the surrounding areas (Figure 1A). No fibrosis was noted in sham or ESAT-6–alone control animals. Comparative fibrosis scoring by the Ashcroft system (19) indicated that MWCNT increased the fibrotic index from 1.5 in C57BL/6 to 4.5 in PPARγ-KO mice ($P < 0.0001$), and MWCNT + ESAT-6 increased the index from 3.4 to 6.3 (C57BL/6 vs. PPARγ-KO; $P < 0.0001$) (Figure 1B).

Additional evaluation of pulmonary fibrotic changes in PPARγ-KO mice was performed by laser capture microdissection analysis of fibronectin gene expression in granuloma-positive versus granuloma-negative regions (Figure 2A). PPARγ-KO mice showed a near doubling of mRNA expression of fibronectin, a characteristic feature of fibrosis (20), in MWCNT + ESAT-6 granuloma-negative compared with granuloma-positive regions. Examination of fibronectin protein by immunostaining of lung tissue sections from each treated group showed increased fibronectin in MWCNT-instilled lung tissue with a further prominent increase around granulomas in MWCNT + ESAT-6–treated mice (Figure 2B). Sham-treated or ESAT-6–instilled lungs revealed minimal fibronectin.

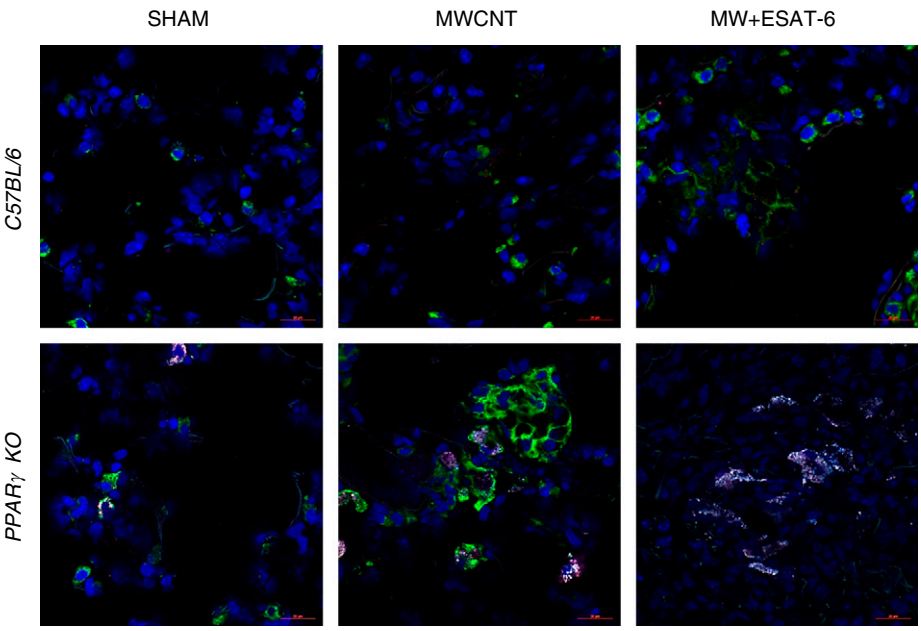

Figure 3. Siglec F expression increases in 60-day PPARγ-KO mice instilled with MWCNT + ESAT-6. Immunofluorescence indicates marked CD11c (green) and minimal Siglec F (red) expression in C57BL/6 mice instilled with MWCNT + ESAT-6. PPARγ-KO macrophages are also CD11c positive with MWCNT, but Siglec F becomes more pronounced after instillation of MWCNT + ESAT-6. Scale bars: 20 μm.

ESAT-6 Increases Macrophage Siglec F Protein Expression in PPARγ-KO Mice

To determine whether ESAT-6 exerted any transformative phenotypic effects on

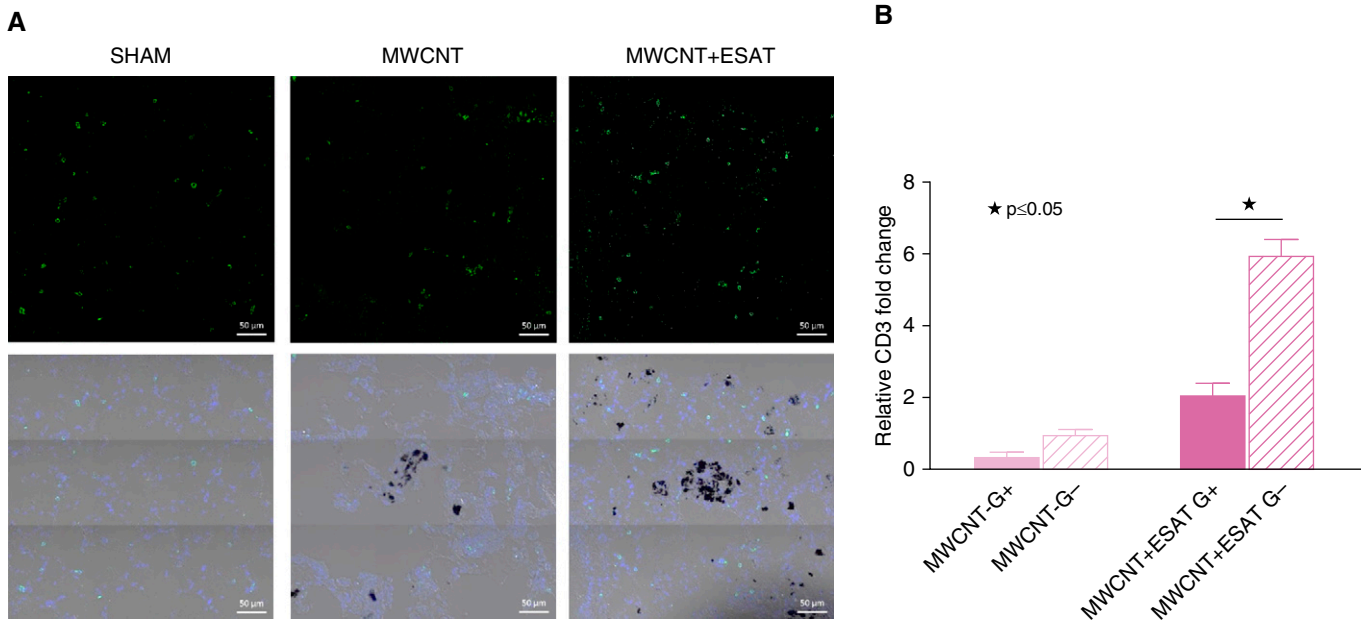

Figure 4. $CD3^+$ T cells are increased in PPARγ-KO mice instilled with MWCNT + ESAT-6. (*A*) Immunofluorescent anti-CD3 staining of lung tissues shows $CD3^+$ cells around the granulomatous region and not within the granuloma itself. Scale bars: 50 μm. (*B*) Laser capture microdissection from lungs of PPARγ-KO mice also shows increased expression of CD3 mRNA in granuloma-negative compared with granuloma-positive regions within the same lung. Reported are the mean ± SEM values for five lungs from each group. ★$P \leq 0.05$.

infiltrating pulmonary macrophages, lung tissues from sham, MWCNT-instilled, and MWCNT + ESAT-6–instilled C57BL/6 and PPARγ-KO mice were immunostained for alveolar macrophage markers CD11c and Siglec F (21). CD11c (green) was expressed on C57BL/6 macrophages with minimal Siglec F (red) expression in both MWCNT and MWCNT + ESAT-6 lung sections (Figure 3). PPARγ-KO macrophages expressed prominent CD11c expression with minimal Siglec F after MWCNT instillation, but after MWCNT + ESAT-6 instillation, Siglec F became more intensely expressed than CD11c (Figure 3), suggesting that ESAT-6 modulated the alveolar macrophage phenotype.

$CD3^+$ Cells Surrounding Granulomas Are Increased in PPARγ-KO Mice Exposed to MWCNT + ESAT-6

We previously reported that in C57BL/6 mice, pulmonary infiltrates of $CD3^+$ lymphocytes were increased around granulomas after instillation of MWCNT + ESAT-6 (15). In the present study, we examined the effects of ESAT-6 on $CD3^+$ infiltration in MWCNT-instilled PPARγ-KO mice. Laser capture microdissection analysis of granuloma-positive and granuloma-negative regions within the same lung indicated that CD3 mRNA expression in PPARγ-KO pulmonary granuloma-negative tissues increased from a mean of 2.1-fold with MWCNT instillation to 6.0-fold after instillation of MWCNT + ESAT-6 (Figure 4B). Immunostaining indicated prominent $CD3^+$ cells within the nongranulomatous regions in MWCNT + ESAT-6–instilled animals compared with MWCNT- or sham-instilled animals (Figure 4A).

Fibrotic Mediator Expression Is Elevated in BAL Cells and BALF

Differential cell counts of PPARγ-KO BAL cells (Table 2) revealed predominately macrophages (ranging from 87% in MWCNT + ESAT-6 to 92% in sham) with elevated lymphocytes and minimal neutrophils (<10%) in all sham and treatment groups. Similarly, BAL of wild-type mice contained 97–99% macrophages but less than 5% lymphocytes. Differential counts of treated groups did not significantly differ from sham for either C57BL/6 or PPARγ-KO mice. Because our previous studies in C57BL/6 mice had detected maximally elevated cytokine expression in BAL cells exposed to MWCNT + ESAT-6 (15), we evaluated BAL cell mRNA responses in PPARγ-KO mice. The results revealed two basic

Table 2. BAL Cell Differentials

Treatment	M	L	PMN
Wild type			
Sham	99 ± 0.6	1 ± 0.6	0
MWCNT	98 ± 2	4 ± 2	0
MWCNT + ESAT-6	97 ± 3	3 ± 3	0
PPARγ-KO			
Sham	92 ± 9	5 ± 4	3 ± 4
MWCNT	88 ± 4	7 ± 3	5 ± 5
MWCNT + ESAT-6	87 ± 5	7 ± 6	7 ± 4

Definition of abbreviations: L = lymphocytes; M = macrophages; PMN = polymorphic nuclear leukocytes; PPARγ-KO = peroxisome proliferator–activated receptor γ–knockout.

patterns of responses in PPARγ-KO mice. For OPN (osteopontin), CCL2, and PDGFa, significant responses ($P \leq 0.05$) were found with either MWCNT alone or MWCNT + ESAT-6 compared with sham treatment (Figures 5A, 5B, and 5E). With IL-13 and matrix metalloproteinase (MMP)-9 (Figures 5F and 5G), significant responses ($P \leq 0.05$) were produced only by combined MWCNT + ESAT-6. Examination of BAL cells from wild-type mice yielded no detectable mRNA responses of either IL-13 or MMP-9 (data not shown).

Interestingly, mRNA expression of TGF-β was not detectable in either PPARγ-KO (Figure 5C) or wild-type mice (data not shown), but PPARγ-KO BAL cells instilled with MWCNT or MWCNT + ESAT-6 expressed elevated levels of the TGF-β signaling gene, Smad3, compared with

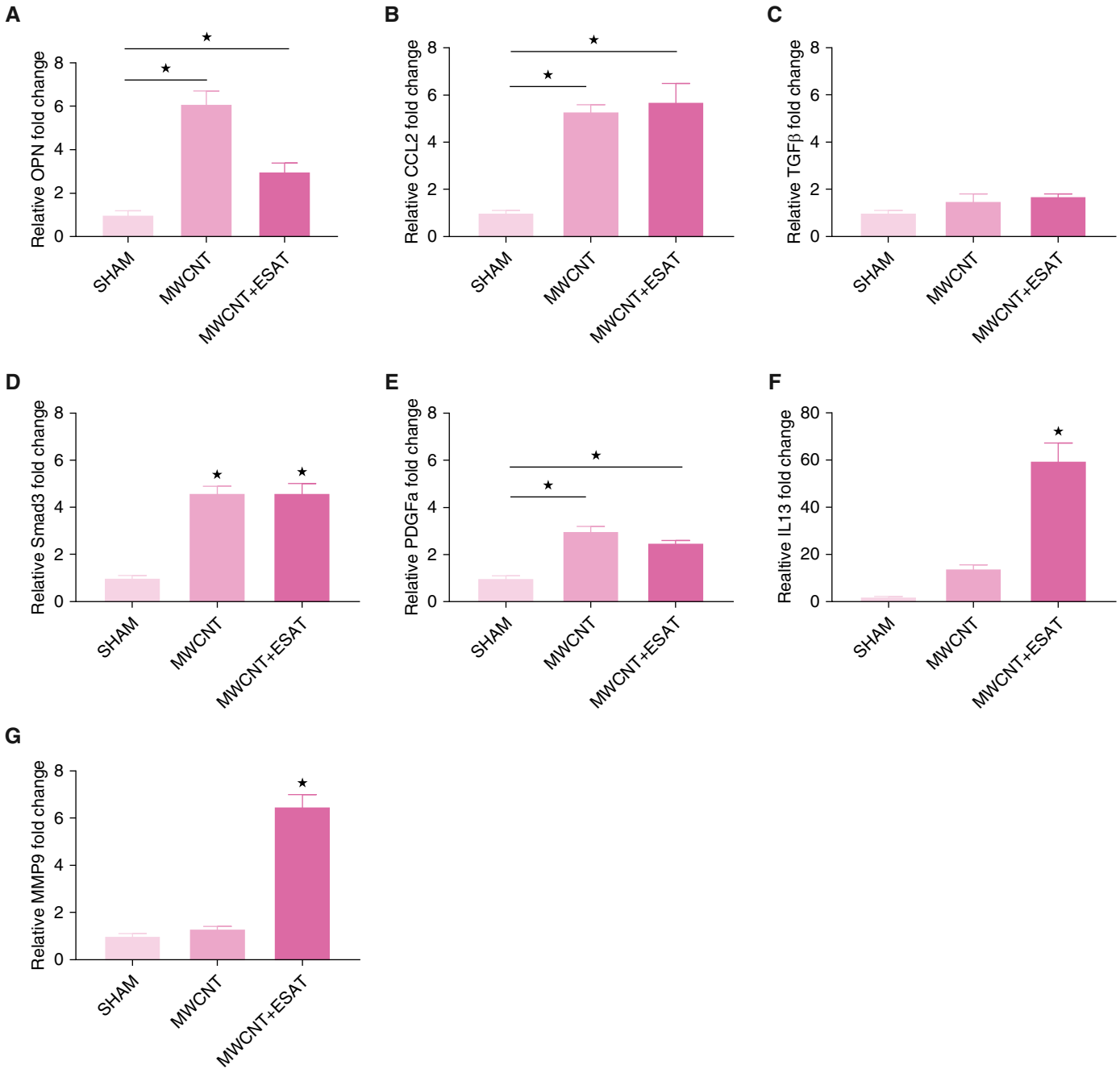

Figure 5. Gene expression from PPARγ-KO BAL cells. (*A*) Osteopontin (OPN) and (*B*) CCL2 were significantly (★$P \leq 0.05$) increased by MWCNT or MWCNT + ESAT-6 instillations compared with sham. (*C*) Transforming growth factor (TGF)-β was not increased by either MWCNT or MWCNT + ESAT-6. (*D*) Smad3 was increased by either MWCNT or MWCNT + ESAT-6 compared with sham (★$P \leq 0.05$). (*E*) Platelet-derived growth factor subunit A (PDGFa) was increased in both treated groups, whereas (*F*) IL-13 and (*G*) matrix metalloproteinase (MMP)-9 were increased only by MWCNT + ESAT-6 instillation compared with sham. Reported are the mean ± SEM values for $n = 4$–10 per group.

sham, suggesting exposure to TGF-β (Figure 5D). Analysis of BALF confirmed this with TGF-β protein levels significantly ($P \leq 0.05$) augmented by MWCNT or MWCNT + ESAT-6 only in BALF from PPARγ-KO mice (Figure 6A) but not from wild-type mice (data not shown). These findings suggested that macrophages were not the only contributors to TGF-β production in PPARγ-KO mice.

A similar pattern was noted with PDGFa protein (Figure 6B), which was significantly elevated ($P \leq 0.05$) versus sham by MWCNT or combined MWCNT + ESAT-6. PDGFa levels induced by the combination were slightly (but not significantly; $P = 0.09$) elevated compared with MWCNT alone (Figure 6B). In contrast, IL-13 protein production was significantly ($P \leq 0.05$) increased by combined MWCNT + ESAT-6 but not by MWCNT alone (Figure 6C). In line with the aforementioned mRNA findings, C57BL/6 BALF levels of IL-13 protein were not detectable (data not shown). C57BL/6, however, did show significant ($P \leq 0.05$) increases in PDGFa protein with either MWCNT (150 pg/ml) or MWCNT + ESAT-6 (155 pg/ml) compared with sham (72 pg/ml). It was noted that PPARγ-KO baseline levels of PDGFa (120 pg/ml) in sham control animals were significantly ($P \leq 0.05$) higher than in wild-type control animals (72 pg/ml).

ESAT-6 Is Retained in Lung Tissues of PPARγ-KO but Not Wild-Type Mice

ESAT-6 is a secreted protein that consists of 95 amino acids. For this study, a modified sequence was used that consists of 15 amino acids starting at position 66 from the full sequence and ending at 80. A nano-LC/MS method was developed and optimized for the detection of the modified ESAT-6 peptide. The nano-LC/MS analysis for ESAT-6 standard is shown in Figure 7A. The extracted ion chromatogram for the $[M + 3H]^{+3}$ at mass-to-charge ratio (m/z) 524.6 Da demonstrates that ESAT-6 is retained on the column until 28.5 minutes (Figure 7A). The first TOF mass spectrometry experiment (Figure 7B) shows the monoisotopic mass measured and calculated to be 1,570.7961 and 1,570.9164 for $[M + 3H]^{+3}$ and $[M + 2H]^{+2}$, respectively. $[M + 3H]^{+3}$ showed less than 1 ppm mass accuracy and was used as the target ion for the analysis of the modified ESAT-6 in lung tissue. The fragmentation pattern for m/z 524.6 Da is shown in Figure 7C, and the peptide fragments identified are listed in Table 3.

The nano-LC/MS analysis was performed because the disparate responses of C57BL/6 and PPARγ-KO mice to ESAT-6 inclusion in the MWCNT instillation protocol suggested that there might be differences in pulmonary retention of ESAT-6. The results indicated an ESAT-6–modified peptide peak was detectable in PPARγ-KO mouse lungs with ESAT-6 alone, as well as with MWCNT + ESAT-6 at 60 days after instillation, and a representative extracted ion chromatogram for m/z Da 524.6 for each group is shown in Figure 7D. Lungs treated with PBS or MWCNT did not provide a detectable peak at 28.5 minutes. ESAT-6 peptide was detected in PPARγ-KO lungs; however, there was no evidence of the peptide in C57BL/6 lungs at 60 days after instillation.

Discussion

Fibrosis is seen in approximately 20–30% of patients with sarcoidosis and is a leading cause of mortality (22). Fibrosis in sarcoidosis follows the same lymphatic distribution as active inflammation (23), and it is presumed that granulomas serve as the nidi for fibrosis (24). Interestingly, our studies in C57BL/6 wild-type and PPARγ-KO mice indicate that ESAT-6 instillation with MWCNT increases both granulomas and fibrosis. Use of Masson's trichrome staining indicated the presence of fibrosis within granulomas and adjacent tissues in the present study and our previous report that focused on ESAT-6 effects in wild-type mice (15).

Fibrotic pathways, however, appear to differ between mouse strains, with TGF-β representing a major component of BALF in PPARγ-KO but not wild-type mice. In line with these findings, in the present study, we also detected elevated Smad3 gene expression in PPARγ-KO BAL cells. TGF-β can be produced by a large number of cell types, such as alveolar macrophages, fibroblasts, and epithelial and endothelial cells (25). In idiopathic pulmonary fibrosis, for example, injured epithelial cells become major producers of TGF-β and engage in profibrotic interactions with fibroblasts (26). Our emphasis has been on the alveolar macrophage, and subsequent studies will be required to delineate the role of epithelial cells in ESAT-6/MWCNT-associated fibrosis.

Maximum levels of TGF-β were noted after ESAT-6 + MWCNT instillation in PPARγ-KO mice. In contrast, TGF-β was virtually undetectable in wild-type mice.

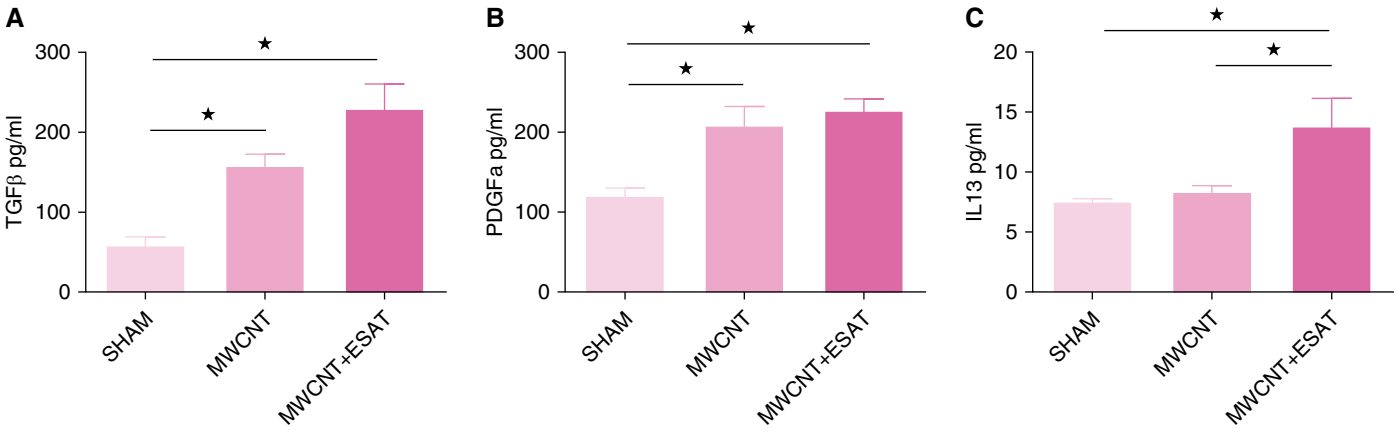

Figure 6. Fibrotic mediator proteins in BAL fluid. (*A*) TGF-β and (*B*) PDGFa proteins are elevated in both MWCNT- and MWCNT + ESAT-6–instilled mice. (*C*) IL-13 is significantly elevated by MWCNT + ESAT-6 only. Reported are the mean ± SEM values of $n = 4–7$ per group. $^{\star}P \leq 0.05$.

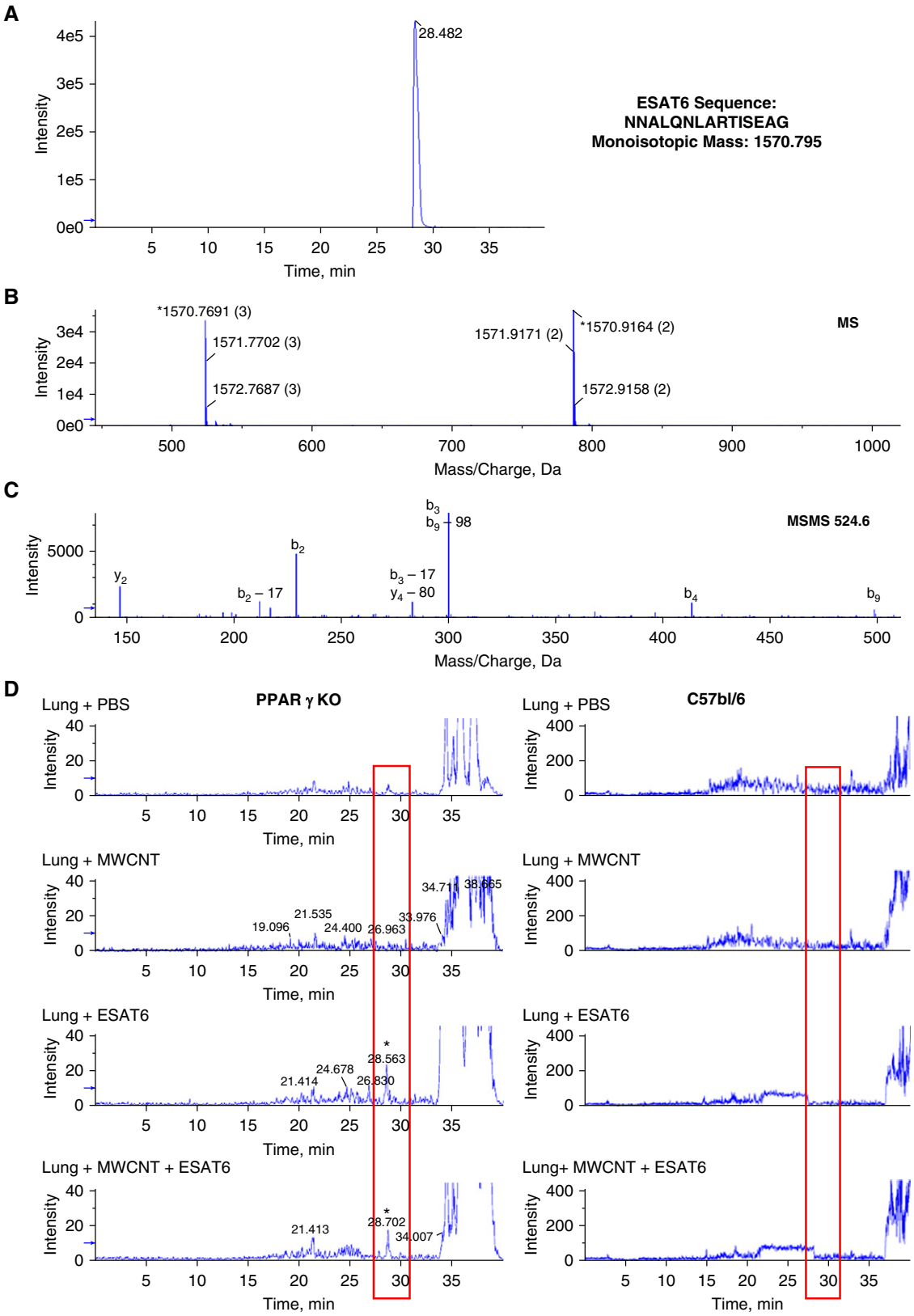

Figure 7. Characterization of modified ESAT-6 using the nano liquid chromatography–mass spectrometry instrument. Mass spectrometry was performed on ESAT-6 standard and homogenates from PPARγ-KO and C57BL/6 lungs. Extracted ion chromatogram for ESAT-6 is retained on the column until 28.5 minutes. (*A*) Full-scan mass spectrometry profile demonstrating the mass (charge state) showing the monoisotopic mass distribution for the $[M + 3H]^{+3}$

Table 3. ESAT-6 Primary Identified Fragment Ions Detected for Mass-to-Charge Ratio 524.6 Da

Name	Charge	m/z	Error (Da)	Sequence
y2	1	147.08	0.02	AG
b2-17	1	212.07	0.02	NN
b2	1	229.09	0.02	NN
b3-17	1	283.10	0.02	NNA
b3	1	300.13	0.02	NNA
b4	1	413.21	0.03	NNAL
b9	2	498.27	0.02	NNALQNLAR

Definition of abbreviation: *m/z* = mass-to-charge ratio.
Data are for ions detected for *m/z* 524.6 Da shown in Figure 7.

Studies in patients with sarcoidosis have suggested that intrinsic alterations in TGF-β may constitute a predisposing factor in developing sarcoidosis-associated pulmonary fibrosis (reviewed by Patterson and colleagues [24]). Production of TGF-β has been shown to be stimulated by IL-13, which also activates functional properties of fibroblasts (27). The present study indicates that in PPARγ-KO but not wild-type mice, the combination of MWCNT + ESAT-6 elicited maximal BAL cell IL-13 mRNA expression as well as IL-13 protein production in BALF. MMP-9, another factor essential to the IL-13/TGF-β pathway (27), was also sharply elevated by MWCNT + ESAT-6 in PPARγ-KO mice. Interestingly, elevated RNA expression of IL-13 has been reported in sarcoidosis BAL cells, and IL-13 protein has been detected in sarcoidosis alveolar macrophages (28, 29). It should also be noted that PPARγ deficiency has also been found in sarcoidosis alveolar macrophages (11). Thus, findings suggest that PPARγ deficiency may promote elevation of factors required for a TGF-β–associated fibrosis pathway that may be suppressed by intact PPARγ activity in wild-type mice.

Elevation of other fibrotic mediators was also noted in PPARγ-KO mice. In contrast to previous studies of C57BL/6 mice (15), OPN and CCL2 were not maximally stimulated by MWCNT + ESAT-6 in PPARγ-KO BAL cells, but expression levels with MWCNT or MWCNT + ESAT-6 were both significantly higher than in sham-treated animals. PDGFa expression showed a similar pattern. OPN, a glycoprotein associated with extracellular matrix changes, has been cited as having multiple roles in fibrosis (30). CCL2, a chemokine capable of inducing fibrocyte recruitment, has also been shown to be necessary for fibrosis induction (31). PDGFa represents a potent mitogen and chemoattractant for lung fibroblasts (20). Both wild-type and PPARγ-KO mice demonstrated significant elevations of PDGFa protein in response to MWCNT + ESAT-6 compared with sham, with slightly lower responses to MWCNT alone. These findings suggest that PDGF fibrotic pathways may differ from those of TGF-β in the lung (32). Of note, significantly higher levels of PDGFa were detected in MWCNT + ESAT-treated PPARγ-KO mice than in C57BL/6 mice. This observation may be related to the presence of endogenous pulmonary inflammation that accompanies PPARγ deficiency (33). Our previous studies have shown that baseline levels of OPN and CCL2 in untreated PPARγ-KO BAL cells are significantly higher than those of wild-type cells, strongly suggesting an endogenous inflammatory condition (17).

In previous reports, we noted that untreated control PPARγ-KO mice exhibited increased lymphocytes in BAL compared with wild-type mice (17, 18). In the present study, we demonstrated an enhanced $CD3^+$ T-cell presence within the lung parenchyma after instillation of MWCNT + ESAT-6 compared with MWCNT alone. $CD3^+$ cells were more frequently detected within nongranulomatous than in granulomatous areas, suggesting that these cells may contribute to the enhanced fibrosis in MWCNT + ESAT-6–treated animals.

Of interest was the finding that ESAT-6 appeared to elevate surface expression of Siglec F on PPARγ-KO but not C57BL/6 alveolar macrophages exposed to MWCNT. Sialic acid–binding immunoglobulin-like lectins (Siglecs) are transmembrane protein members of the immunoglobulin superfamily (34) with predominantly inhibitory functions. Siglec F is a marker for murine alveolar macrophages (21), and the inhibitory motifs are located in the cytoplasmic domain (34). Siglec–ligand interactions are required to regulate immune cell functions, but the biological context in which Siglecs function is still not well understood (35). The elevation of Siglec F by ESAT-6 has not been reported previously, and although it appears as if PPARγ-KO alveolar macrophages may express some immune-inhibitory activity, additional studies will be required to confirm this.

Finally, one of the most surprising findings in this study was the lack of ESAT-6 persistence in lungs of wild-type mice versus PPARγ-KO animals at 60 days after instillation of ESAT-6 alone or MWCNT + ESAT-6. A characteristic function of PPARγ is to enhance macrophage phagocytosis of cellular or bacterial debris as part of a general effect to resolve inflammation, suggesting that the intact phagocytic functioning in wild-type mice might be responsible for removing ESAT-6 debris (36). Despite persistence of ESAT-6 alone, ESAT-6 had no effect on pathophysiology in either mouse strain; yet, ESAT-6 combined with MWCNT clearly elicited inflammatory and fibrotic mediators in both strains. Earlier studies have demonstrated a synergistic effect of nanotubes or environmental pollutants on immune reactivity when a second insult such as allergens or infectious agents is provided (37, 38). Our studies have demonstrated that alterations in lymphocyte populations after the first insult are compounded by further perturbations.

Figure 7. (Continued). and $[M + 2H]^{+2}$ ions (*B*) and MSMS fragmentation pattern for the $[M + 3H]^{+3}$ at mass-to-charge ratio (*m/z*) 524.6 Da ion with the identified fragment ions listed in Table 3 (*C*). (*D*) Extracted ion chromatograms for *m/z* 524.6 Da for the ESAT-6 $[M + 3H]^{+3}$ ion in PPARγ-KO and C57BL/6 lungs instilled with PBS, MWCNT, ESAT-6, or MWCNT + ESAT-6. The ESAT-6–modified peptide peak was detected in the lungs with ESAT-6 and MWCNT + ESAT-6 after 60 days, and a representative extracted ion chromatogram for m/z 524.6 for each group is shown in *D*. The lungs treated with PBS or MWCNT did not provide a detectable peak at 28.5 minutes. ESAT-6 peptide was not detectable in lungs from C57BL/6 mice.

Future nanotube studies will be required to determine whether innate and/or adaptive immune system reactivity is altered by ESAT-6 inclusion.

Conclusions

The data derived from the present study indicate that PPARγ deficiency promotes pulmonary ESAT-6 retention, exacerbates macrophage responses to MWCNT + ESAT-6, and intensifies pulmonary fibrosis. The findings suggest that the MWCNT model may facilitate better understanding of the effects of environmental factors on sarcoidosis-associated pulmonary fibrosis. Instillation of mycobacterial ESAT-6 peptide with MWCNT into PPARγ-KO mice appears to exacerbate inflammatory and fibrotic pathways, some of which have been documented in sarcoidosis. The absence of available clinical interventions directed against sarcoidosis-associated pulmonary fibrosis, however, means that lung transplant is the only option for these patients. A reliable murine model of fibrosis will allow better understanding of the pathophysiology of sarcoidosis and the influences of environmental triggers such as CNTs and bacterial products on pulmonary fibrogenesis. ■

Author disclosures are available with the text of this article at www.atsjournals.org.

References

1. Pietroiusti A, Stockmann-Juvala H, Lucaroni F, Savolainen K. Nanomaterial exposure, toxicity, and impact on human health. *Wiley Interdiscip Rev Nanomed Nanobiotechnol* [online ahead of print] 23 Feb 2018; DOI: 10.1002/wnan.1513.
2. Lam CW, James JT, McCluskey R, Arepalli S, Hunter RL. A review of carbon nanotube toxicity and assessment of potential occupational and environmental health risks. *Crit Rev Toxicol* 2006;36:189–217.
3. Wu M, Gordon RE, Herbert R, Padilla M, Moline J, Mendelson D, *et al*. Case report: lung disease in World Trade Center responders exposed to dust and smoke. Carbon nanotubes found in the lungs of World Trade Center patients and dust samples. *Environ Health Perspect* 2010;118:499–504.
4. Kolosnjaj-Tabi J, Just J, Hartman KB, Laoudi Y, Boudjemaa S, Alloyeau D, *et al*. Anthropogenic carbon nanotubes found in the airways of Parisian children. *EBioMedicine* 2015;2:1697–1704.
5. Murray AR, Kisin ER, Tkach AV, Yanamala N, Mercer R, Young SH, *et al*. Factoring-in agglomeration of carbon nanotubes and nanofibers for better prediction of their toxicity versus asbestos. *Part Fibre Toxicol* 2012;9:10.
6. Hamilton RF Jr, Wu Z, Mitra S, Shaw PK, Holian A. Effect of MWCNT size, carboxylation, and purification on in vitro and in vivo toxicity, inflammation and lung pathology. *Part Fibre Toxicol* 2013; 10:57.
7. Newman LS, Rose CS, Bresnitz EA, Rossman MD, Barnard J, Frederick M, *et al*.; ACCESS Research Group. A case control etiologic study of sarcoidosis: environmental and occupational risk factors. *Am J Respir Crit Care Med* 2004;170:1324–1330.
8. Prezant DJ, Dhala A, Goldstein A, Janus D, Ortiz F, Aldrich TK, *et al*. The incidence, prevalence, and severity of sarcoidosis in New York City firefighters. *Chest* 1999;116:1183–1193.
9. Crowley LE, Herbert R, Moline JM, Wallenstein S, Shukla G, Schechter C, *et al*. "Sarcoid like" granulomatous pulmonary disease in World Trade Center disaster responders. *Am J Ind Med* 2011;54:175–184.
10. Huizar I, Malur A, Midgette YA, Kukoly C, Chen P, Ke PC, *et al*. Novel murine model of chronic granulomatous lung inflammation elicited by carbon nanotubes. *Am J Respir Cell Mol Biol* 2011;45:858–866.
11. Culver DA, Barna BP, Raychaudhuri B, Bonfield TL, Abraham S, Malur A, *et al*. Peroxisome proliferator–activated receptor gamma activity is deficient in alveolar macrophages in pulmonary sarcoidosis. *Am J Respir Cell Mol Biol* 2004;30:1–5.
12. Barna BP, McPeek M, Malur A, Fessler MB, Wingard CJ, Dobbs L, *et al*. Elevated microRNA-33 in sarcoidosis and a carbon nanotube model of chronic granulomatous disease. *Am J Respir Cell Mol Biol* 2016; 54:865–871.
13. Mohan A, Malur A, McPeek M, Barna BP, Schnapp LM, Thomassen MJ, *et al*. Transcriptional survey of alveolar macrophages in a murine model of chronic granulomatous inflammation reveals common themes with human sarcoidosis. *Am J Physiol Lung Cell Mol Physiol* 2018;314:L617–L625.
14. Oswald-Richter KA, Culver DA, Hawkins C, Hajizadeh R, Abraham S, Shepherd BE, *et al*. Cellular responses to mycobacterial antigens are present in bronchoalveolar lavage fluid used in the diagnosis of sarcoidosis. *Infect Immun* 2009;77:3740–3748.
15. Malur A, Barna BP, Patel J, McPeek M, Wingard CJ, Dobbs L, *et al*. Exposure to a mycobacterial antigen, ESAT-6, exacerbates granulomatous and fibrotic changes in a multiwall carbon nanotube model of chronic pulmonary disease. *J Nanomed Nanotechnol* 2015; 6:340.
16. Drake WP, Dhason MS, Nadaf M, Shepherd BE, Vadivelu S, Hajizadeh R, *et al*. Cellular recognition of *Mycobacterium tuberculosis* ESAT-6 and KatG peptides in systemic sarcoidosis. *Infect Immun* 2007;75: 527–530.
17. Huizar I, Malur A, Patel J, McPeek M, Dobbs L, Wingard C, *et al*. The role of PPARγ in carbon nanotube-elicited granulomatous lung inflammation. *Respir Res* 2013;14:7.
18. Malur A, Mccoy AJ, Arce S, Barna BP, Kavuru MS, Malur AG, *et al*. Deletion of PPAR γ in alveolar macrophages is associated with a Th-1 pulmonary inflammatory response. *J Immunol* 2009;182: 5816–5822.
19. Hübner RH, Gitter W, El Mokhtari NE, Mathiak M, Both M, Bolte H, *et al*. Standardized quantification of pulmonary fibrosis in histological samples. *Biotechniques* 2008;44:507–511, 514–517.
20. Kolahian S, Fernandez IE, Eickelberg O, Hartl D. Immune mechanisms in pulmonary fibrosis. *Am J Respir Cell Mol Biol* 2016;55:309–322.
21. Misharin AV, Morales-Nebreda L, Mutlu GM, Budinger GR, Perlman H. Flow cytometric analysis of macrophages and dendritic cell subsets in the mouse lung. *Am J Respir Cell Mol Biol* 2013;49: 503–510.
22. Lopes AJ, de Menezes SL, Dias CM, de Oliveira JF, Mainenti MR, Guimarães FS. Comparison between cardiopulmonary exercise testing parameters and computed tomography findings in patients with thoracic sarcoidosis. *Hai* 2011;189:425–431.
23. American Thoracic Society. Statement on sarcoidosis: joint statement of the American Thoracic Society (ATS), the European Respiratory Society (ERS) and the World Association of Sarcoidosis and Other Granulomatous Disorders (WASOG) adopted by the ATS Board of Directors and by the ERS Executive Committee, February 1999. *Am J Respir Crit Care Med* 1999; 160:736–755.
24. Patterson KC, Hogarth K, Husain AN, Sperling AI, Niewold TB. The clinical and immunologic features of pulmonary fibrosis in sarcoidosis. *Transl Res* 2012;160:321–331.
25. Fernandez IE, Eickelberg O. The impact of TGF-β on lung fibrosis: from targeting to biomarkers. *Proc Am Thorac Soc* 2012;9:111–116.
26. Sakai N, Tager AM. Fibrosis of two: epithelial cell-fibroblast interactions in pulmonary fibrosis. *Biochim Biophys Acta* 2013;1832:911–921.
27. Lee CG, Homer RJ, Zhu Z, Lanone S, Wang X, Koteliansky V, *et al*. Interleukin-13 induces tissue fibrosis by selectively stimulating and activating transforming growth factor β1. *J Exp Med* 2001; 194:809–821.
28. Hauber HP, Gholami D, Meyer A, Pforte A. Increased interleukin-13 expression in patients with sarcoidosis. *Thorax* 2003;58:519–524.
29. Hancock A, Armstrong L, Gama R, Millar A. Production of interleukin 13 by alveolar macrophages from normal and fibrotic lung. *Am J Respir Cell Mol Biol* 1998;18:60–65.
30. Dong J, Ma Q. Osteopontin enhances multi-walled carbon nanotube-triggered lung fibrosis by promoting TGF-β1 activation and myofibroblast differentiation. *Part Fibre Toxicol* 2017;14:18.

31. Sun L, Louie MC, Vannella KM, Wilke CA, LeVine AM, Moore BB, *et al*. New concepts of IL-10-induced lung fibrosis: fibrocyte recruitment and M2 activation in a CCL2/CCR2 axis. *Am J Physiol Lung Cell Mol Physiol* 2011;300:L341–L353.
32. Deng X, Jin K, Li Y, Gu W, Liu M, Zhou L. Platelet-derived growth factor and transforming growth factor β1 regulate ARDS-associated lung fibrosis through distinct signaling pathways. *Cell Physiol Biochem* 2015;36:937–946.
33. Gautier EL, Chow A, Spanbroek R, Marcelin G, Greter M, Jakubzick C, *et al*. Systemic analysis of PPARγ in mouse macrophage populations reveals marked diversity in expression with critical roles in resolution of inflammation and airway immunity. *J Immunol* 2012;189:2614–2624.
34. Feng YH, Mao H. Expression and preliminary functional analysis of Siglec-F on mouse macrophages. *J Zhejiang Univ Sci B* 2012;13: 386–394.
35. Macauley MS, Crocker PR, Paulson JC. Siglec-mediated regulation of immune cell function in disease. *Nat Rev Immunol* 2014;14: 653–666.
36. Croasdell A, Duffney PF, Kim N, Lacy SH, Sime PJ, Phipps RP. PPARγ and the innate immune system mediate the resolution of inflammation. *PPAR Res* 2015;2015:549691.
37. Provoost S, Maes T, Willart MA, Joos GF, Lambrecht BN, Tournoy KG. Diesel exhaust particles stimulate adaptive immunity by acting on pulmonary dendritic cells. *J Immunol* 2010;184: 426–432.
38. Matthews NC, Pfeffer PE, Mann EH, Kelly FJ, Corrigan CJ, Hawrylowicz CM, *et al*. Urban particulate matter-activated human dendritic cells induce the expansion of potent inflammatory Th1, Th2, and Th17 effector cells. *Am J Respir Cell Mol Biol* 2016;54: 250–262.